https://doi.org/10.1016/j.apenergy.2020.115215 **This is the Pre-Published Version.**

# Experimental study on wind speeds in a complex-terrain wind farm and analysis of wake effects

Haiying Sun[a*], Xiaoxia Gao[b], Hongxing Yang[a*]

[a]Renewable Energy Research Group, Department of Building Services Engineering, The Hong Kong Polytechnic University, Hong Kong

[b]Department of Power Engineering, North China Electric Power University (Baoding), Baoding, PR China

**Abstract**

In this paper, wind speed deficits have been quantified based on the field observations from the hilly Shiren wind farm in China. Two lidars have been applied to measure wind speeds in the wind farm. Two clusters of wind turbines in different layout patterns were chosen for the experiments. One cluster was the upstream-and-downstream pattern, which was used to investigate the upstream turbine's wake impact on the downstream turbine. According to the experiment, the wake width of the downstream turbine widened and the largest wind speed deficit decreased gradually in the downstream direction. Meanwhile, the wake centerlines of upstream and downstream wind turbines were subjected to the wind direction and may not be in the same line. The other cluster was the side-by-side pattern, which was to investigate how the wakes and the wake interactions develop downwind of a row of wind turbines. It has been found that huge wind speed deficits existed behind the wind turbines. The wind speeds reduced mostly from 14.4 m/s to 8.0 m/s in the downwind direction and from 12.4 m/s to 4.2 m/s in the crosswind direction. Wind speeds were not stable in the far-wake zone. The wake boundary was not easy to determine as well. When wakes of two adjacent turbines encountering, the interaction effect became complicated. In these experiments, the complex terrain is one of the most important factors that complicates the wake distribution. Therefore, the influence of the terrain shape on wake distribution should be continuously investigated in the future.

Keywords: Wind field experiments; Complex-terrain wind farm; Wake effect; Upstream-and-downstream pattern; Side-by-side pattern.

## 1. Introduction

Wind is one of the most profitable renewable energy sources all over the world [1]. The

* Corresponding author. Tel: Haiying Sun: 2766 4815; Hongxing Yang: 2766 5863

*E-mail address:* Haiying Sun: haiying.sun@connect.polyu.hk; Hongxing Yang: hong-xing.yang@polyu.edu.hk

The short version of the paper was presented at Applied Energy Symposium: MIT A+ B, May 22-24, Boston. This paper is a substantial extension of the short version of the conference paper.

wake effect is a complex phenomenon that exists downwind of operating wind turbines [2]. It is related to the wind turbines [3], the layout of the wind farm [4], and the characteristics of the atmosphere [5]. Wake interferences between wind turbines have important influence on wind farms [6]. Understanding the wind deficits caused by wakes is significant in wind engineering [7]. One of the most effective ways to study the wake effect is by analyzing the wind data in operating wind farms [8]. Comprehensive and accurate wake measurements are also essential for developing and validating advanced wind farm models [9]. In terms of optimizing the layout of a wind farm, it is of great significance to understand the turbulence development and power losses due to wake interactions [10]. Recently, with the rapid development of the wind energy industry, the wake data from full-scale experiments are particularly needed. However, there are still no enough wake data from the field experiments yet. It is a very difficult and time-consuming task to characterize the entire wind field by measuring the wake effect [11]. The equipment cost and the staff cost make wind field experiments very expensive. More importantly, huge technical difficulties exist in deciding the appropriate lidar scanning strategy and effectively integrating measured data from various remote sensing platforms [12].

The history of measuring wake effect in onshore wind farms has been more than thirty-five years so far. As early as the year of 1982, a field measurement was conducted for three MOD-2 wind turbines situated at Goodnoe Hills, Washington [13]. The objective was to determine the deficit of wind velocity in the centerline and its downwind development under different meteorological conditions. In 1992, a detailed measuring campaign was organized in the Sexbierum Wind Farm in the Netherlands [14]. The experiment aimed at collecting data on wind speed, turbulence intensity, and shear stress at several downwind distances of a wind turbine. Next, the flat-terrain Nørrekær Enge wind farm [15] was used to validate the effectiveness of WindFarmer software in predicting the power reduction of the wake affected turbines in rows with varying spacings. MacHielse, et al. [16] collected two-year measurement data from the ECN Wind Turbine Test Station Wieringermeer, which was situated in a flat open farmland in the Netherlands. Some other tested data were used to validate models for simulating wakes and designing wind farms. For example, a series of CWEX experiments were conducted in the wind farm in central Iowa from 2010 to 2013 [17]. CWEX-10 and CWEX-11 experiments revealed the influence of one-row wind turbines on the local environment [18]. CWEX-13 campaign demonstrated frequent nocturnal low-level jets and strong diurnal cycles of atmospheric stability [19]. The Risø test field is located at a relatively homogeneous terrain in Roskilde, Denmark. Based on the experiments in this wind farm, Bingöl, et al. [20] developed a measurement technique to directly measure the instantaneous wake effect. Then, Trujillo, et al. [9] dealt with the analysis of the two-dimensional wake measurements, which enabled to

estimate the wind speed in the vertical sections perpendicular to the rotor axis. Zhao, et al. [21] studied the wake characteristics of wind turbines with different rotor diameters and their wake interactions. Besides, some remote sensing measurements were focused on wake validations of individual isolated wind turbines rather than wind farms.

Offshore wind power develops rapidly, which represents the most promising renewable energy [22]. For offshore wind farms, wind losses and enhanced loads caused by the wake effect are particularly high [3]. A series of offshore wind farm measurement campaigns were conducted in Vindeby, Denmark, where a ship-mounted sodar was used to measure the wakes. Barthelmie, et al. [23] assessed the applicability of mounting a sodar on a ship and investigated the impact of the wind turbine noise on the vertical wind velocity profile measured by the sodar. Then, Barthelmie, et al. [24] evaluated six wake models through a series of experiments. The wake models were used to measure and predict wakes downstream of a wind turbine, including Risø engineering model [25], Risø WAsP model [26], Risø analytical model [27], UO FLaP model [28], ECN Wakefarm model [29], and RGU computational fluid dynamics model [30]. The analysis illustrated that some models tended toward high or low prediction, but this was not completely consistent. The Horns Rev wind farm in the North Sea is also a large offshore wind farm exposed to low turbulence flow. Jensen, et al. [31] studied the recovery of its inner wake flow. The study was helpful for the development of advanced engineering and scientific models for analyzing the external wakes of the offshore wind farm. Barthelmie, et al. [32] then analyzed the data from the Horns Rev wind farm in the year 2005 and compared various models. With the measurement data, the models were validated and improved in terms of predicting the power losses caused by wakes. Another offshore wind farm experiment was conducted in the Middelgrunden wind farm, which was installed in the Øresund strait, between Denmark and Sweden. Based on the measured data, Barthelmie, et al. [33] described two methods for estimating turbulence intensity. It was found that the simulations were in good agreement with the observations and the turbulence increased by approximately 20% for the flow along the row [34].

In recent years, significant progress has proved that it is complicated to extract robust and quantitative metrics of wake characteristics, such as length scale and velocity deficit [35]. In complex terrains, the issues of wake characterization are further enlarged [36]. The wake behavior has a close relationship to both the flow and the terrain slope [37]. One of the first measurements of wind turbine wakes using lidar in the relatively complex terrain was involved in the Perdigão experiment [36]. The site of the wind farm is formed by two parallel ridges that measure about 4 km lengthwise. The hills are steep, with the valley-to-peak height of more than

200 m and the inclination of approximately 35 % [37]. Barthelmie, et al. [36] described wake measurements with lidars and investigated the advantages of data integration from various scanning strategies as well.

So far, the characteristics of wakes in complex terrains have not been well understood yet, and no enough wind field data could be used on this problem either. Therefore, in the work described herein, we focus on the measurements in the complex-terrain wind fields. In Chapter 2, the site and layout of the tested wind farm are described in detail. In Chapter 3, the measuring equipment, including one anemometer tower and two lidars applied in the experiments are introduced. In Chapter 4, experiments of two clusters of wind turbines in different layout patterns are introduced. The experimental data are analyzed and discussed. Finally, in Chapter 5, the conclusions of this study are drawn. The work described in this paper will not only provide the first-hand measurements from the wind field, but also give guidance on wind field experiments for the future study.

## 2. Site and layout of the Shiren wind farm

The experiments have been conducted in the Shiren Wind Farm, which belongs to Hebei Longyuan Wind Power Co., LTD. The wind farm is located in Shangyi Country, Zhangjiakou City, Hebei Province, China [38]. The power booster station is located at 40.985833° N, 114.361667° E, and the altitude is 1814 m. The terrain of the wind farm is characterized by low mountains and hilly areas [39]. The location of the Shiren Wind Farm is shown in Figure 1.


Figure 1 Location of the Shiren Wind Farm.

Shiren Wind Farm has a capacity of 75 MW. The wind farm consists of 50 numbers of 1.5 MW wind turbines, of which 33 are AW77-1500 type and 17 are UP77-1500 type [40]. For the AW77-1500 type wind turbine, the rotor diameter is 77 m and the hub height is 60 m. For the

UP77-1500 type wind turbine, the rotor diameter is 77 m and the hub height is 65 m. The layout pattern of wind turbines in Shiren Wind Farm is shown in Figure 2.

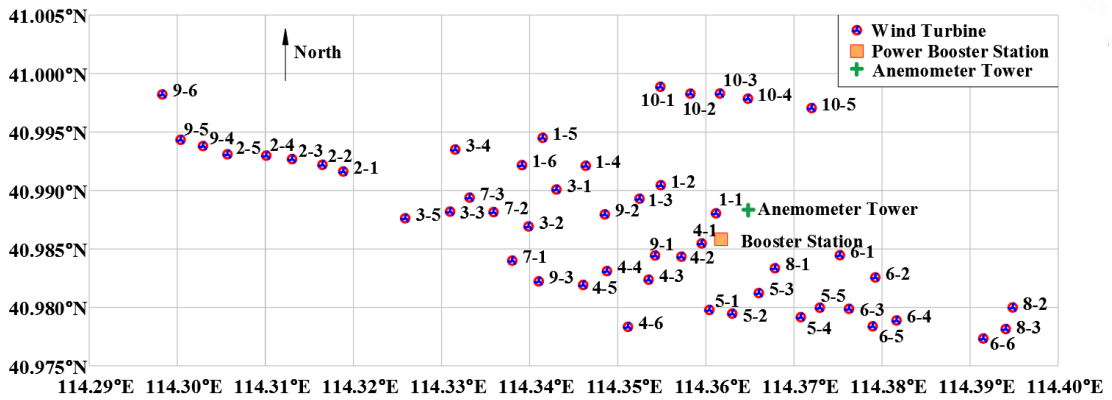


Figure 2 The layout pattern of wind turbines in the Shiren Wind Farm.

Shiren Wind Farm is built in a hilly area with the maximum altitude difference of 171.3 m. Among all wind turbines, the highest one is WT10-5, with an altitude of 1894.1 m; whereas the lowest one is WT8-2, with an altitude of 1722.8 m. This wind farm is a good representative of complex-terrain wind farms. The first-hand wind speed data published in this paper will contribute to both the research study and the engineering application in the complex-terrain wind farms.

## 3. Introduction of measuring equipment

### 3.1 Anemometer tower in wind farm

The wind farm has an anemometer tower at an altitude of 1807.5 m. The location of the tower is 40.988352° N, 114.364810° E. It uses hemispherical cup anemometers to measure wind velocity at 10 m and 65 m heights. At each measuring height, an anemometer and a wind vane are applied to measure wind speed and wind direction, respectively. Figure 3 shows the anemometer tower and the measuring equipment at a height of 10 m.

(a)  (b) 

Figure 3 The anemometer tower: (a) the anemometer tower testing in the field; and (b) the measuring equipment at 10m height.

The data obtained from the anemometer tower provide the evidence for estimating and arranging the power output of a wind farm. However, the anemometer tower cannot monitor the inflow of each wind turbine at different heights.

For the wake study, the awareness of the accurate upstream and downstream wind distributions is of extreme importance. Therefore, two moveable lidars were used in the experiments, which could measure the inflow and wakes of the target wind turbines more accurately.

### 3.2 WindMast WP350

WindMast WP350 and Wind3D 6000 are the two lidars mentioned above, which were rented from QINGDAO Leice Transient Technology Co. LTD. The two wind lidars adopt the non-contact measurement and the target motion is not disturbed. Atmospheric wind field is the main factor that drives the atmospheric circulation, material transportation, and weather phenomena of various scales. Both two lidars can be used in complex terrains, as long as the laser beam is not blocked. One thing to note is that though lidars could be placed in inhomogeneous sites, they must be positioned horizontally. Therefore, before the actual experiments, the two lidars were calibrated by the data from the anemometer tower.

WindMast WP350 is a vertical lidar designed to replace wind towers. It has relatively high precision and requires low power consumption. The wind speed and wind profile of any 30 height gates from 20 m to 350 m above the lidar can be continuously detected throughout the day. The speed range is from 0 to 75 m/s, with the error smaller than 0.1 m/s. The technical

specifications of WindMast WP350 could be found in reference [39]. The WP350 used in the experiments is shown in Figure 4.

(a)  (b) 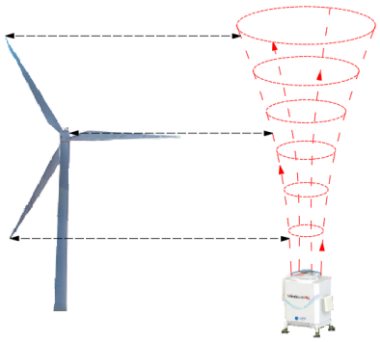

Figure 4 Demonstration of WindMast WP350: (a) WP350 testing in the field; and (b) the scan range.

### 3.3 Wind3D 6000

Wind3D 6000 is a three-dimensional (3-D) scanning wind lidar, which can realize the detection of 3-D wind fields in the middle and lower troposphere, including the atmospheric boundary layer. It has several scanning modes. The radial detection range is from 45 m to 6 km and the speed error is also smaller than 0.1 m/s. Wind3D 6000 meets the requirements of wind turbine wake measurement in complex-terrain wind fields. The technical specifications of Wind3D 6000 could be found in reference [39]. The device applied in the experiments is shown in Figure 5.

(a)  (b) 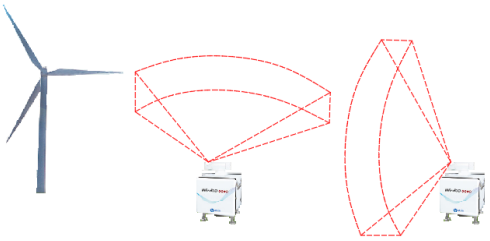

Figure 5 Demonstration of Wind3D 6000: (a) Wind3D 6000 testing in the field; and (b) the scan modes.

## 4. Experimental results and analysis

The lidars were firstly calibrated by comparing the measurements with the wind speed

measured from the anemometer tower at the same location. Then the lidars were applied in measurements of two clusters of turbines of different layout patterns. One cluster is the upstream-and-downstream layout pattern and the other one is the side-by-side layout pattern.

## 4.1 Two wind turbines in the upstream-and-downstream pattern

In this experiment, WT1-4 and WT9-2 were selected as the target turbines for investigating the influence of the upstream wind turbine on the downstream wind turbine. Two turbines were chosen with full consideration of both the prevailing wind directions and the obstacles in the wind field. The positions of wind turbines and lidars are shown in Table 1.

Table 1 Positions of wind turbines and lidars in the upstream-and-downstream pattern experiment

| | **WT1-4** | **WT9-2** | **Wind3D 6000** | **WP350** |
|---|---|---|---|---|
| Longitude | 114.346372˚ E | 114.348533˚ E | 114.351035˚ E | 114.346302˚ E |
| Latitude | 40.992113˚ N | 40.987956˚ N | 40.978225˚ N | 40.993514˚ N |
| Altitude | 1794.6 m | 1800.6 m | 1819.6 m | 1766.2 m |

Plan Position Indicator (PPI) was applied to investigate the interaction of wind turbine wakes. When scanning in PPI mode, the lidar holds its elevation angle constant but varies its azimuth angle. If the lidar rotates through 360 degrees, the scan is called a *surveillance scan*. In this study, the surveillance scan was not necessary, therefore Wind3D 6000 only performed a sector scan, which means it rotated less than 360 degrees.

The prevailing wind directions of the wind farm were between north and northwest. Data were collected when WT9-2 was right under the wake effect of WT1-4. The positions of lidars and two measured wind turbines are demonstrated in Figure 6. The sector enclosed by red lines represents the scanning area of Wind3D 6000.

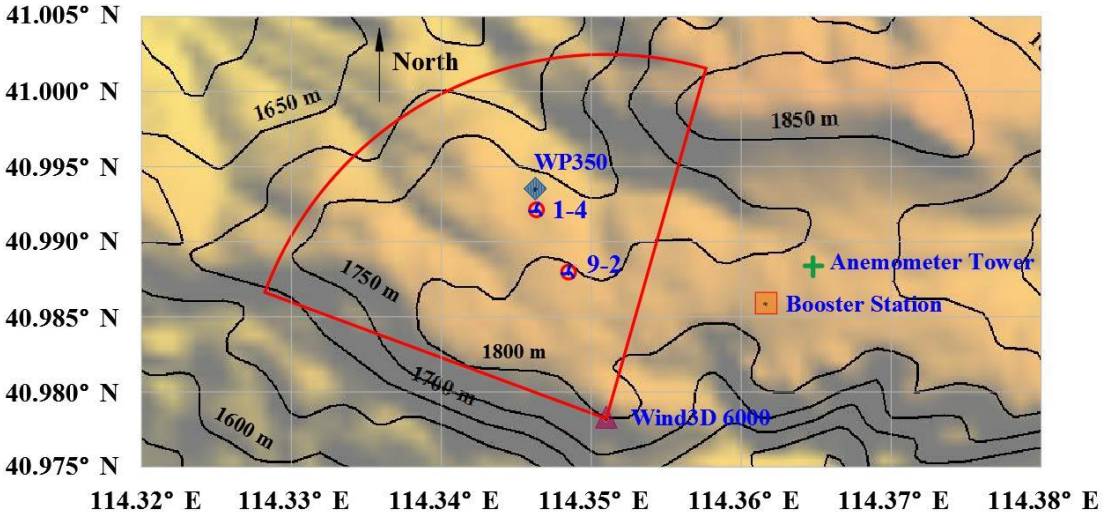


Figure 6 The positions of lidars and wind turbines in the upstream-and-downstream pattern experiment.

In the experimental period, wind directions were changing all the time. Therefore, the effective results must be carefully selected from all measured data. To be specific, WT9-2 must be in the wake-influenced area of WT1-4 and the stable wind should last long enough for lidars to measure the wind data. Also, the aerosol concentration must be within the operating ranges of lidars, which means the air should neither be too dirty nor too clean. Figure 7 demonstrates the schematic diagram of WP350 testing in the field. WT1-4 is enclosed by the yellow line, whereas WP350 is enclosed by the red line.

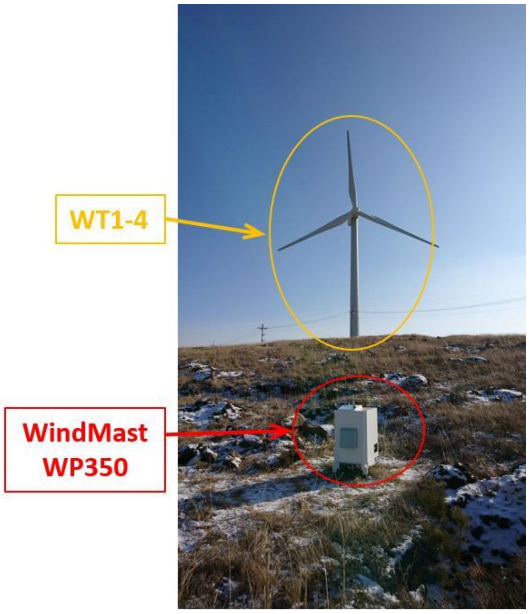


Figure 7 Schematic diagram of WindMast WP350 testing in the field.

The inflow wind speeds and wind directions measured by WP350 in the selected periods are shown in Figure 8. Three qualified periods have been chosen, which are: Time 1: 17:16, March 3rd, 2019; Time 2: 17:29, March 3rd, 2019; and Time 3: 8:33, March 5th, 2019. The wind directions changed in the range of 310° to 340°. The winds were highly centralized, which helped to obtain the specific wake effect.

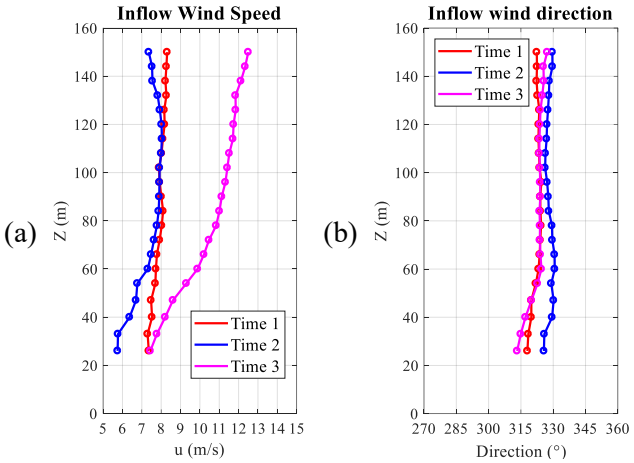


Figure 8 Inflow wind of the upstream-and-downstream pattern experiment: (a) wind speed; and (b) wind direction.

The wind speeds measured by Wind3D 6000 are shown in Figure 9. Apart from WT1-4 and WT9-2, several other wind turbines were also in the scanning zone, where the wind speeds are blank in figures. The wind speeds near the turbines could not be detected, because the turbines interfered with the wind speed measurement surround themselves. WT1-4 and WT9-2 are marked with black dots. In those moments, WT9-2 was partly under the wake effect of WT1-4.

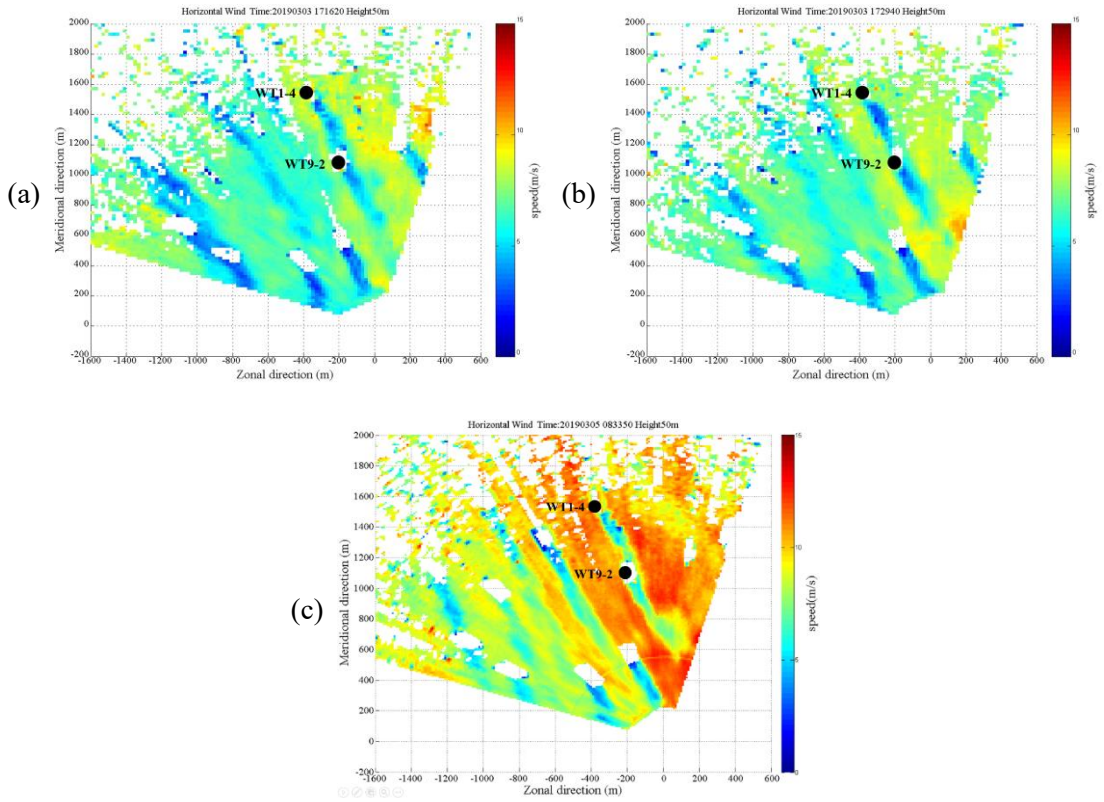


Figure 9 PPI scanning results in the plane through the hub height of WT1-4 (the upstream-and-downstream pattern experiment): (a) Time 1; (b) Time 2; and (c) Time 3.

To quantitatively analyze the wake effect, the wind speed data were filtered based on analyzing lines, as shown in Figure 10. Line 1, Line 2, Line 3, and Line 4 are in the direction of the wake development. To be specific, Line 2 passes through WT1-4 and WT9-2. The other three lines are parallel to Line 2. The spacing between every two adjacent lines is 1/2D (D represents the rotor diameter of the wind turbine). The Baseline is perpendicular to Line 2 and passes through WT1-4, which is applied to study the wake effect in the crosswind sections. Line_U2D to Line_U6D are five lines defined to analyze the wind speed downstream of WT1-4. The distance from WT1-4 to Line_U2D is 2D, and the spacing between any other two adjacent lines is 1D. Similarly, Line_D2D to Line_11D are ten lines to analyze the wind speed downstream of WT9-2. The distance from WT9-2 to Line_D2D is 2D, and the spacing between any other two adjacent lines is 1D as well.

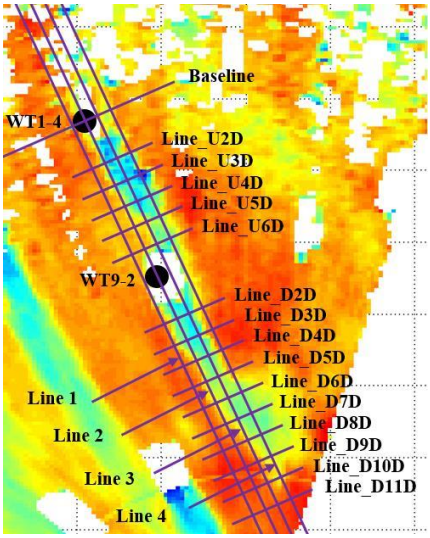


Figure 10 Diagram of analyzing lines of the upstream-and-downstream pattern experiment.

The wind speeds and the altitudes of the four mentioned analyzing lines are demonstrated in Figure 11. The relative positions of WT1-4 and WT9-2 are shown in the figure as well. The distance from WT1-4 to WT9-2 is 6.4D.

(a)

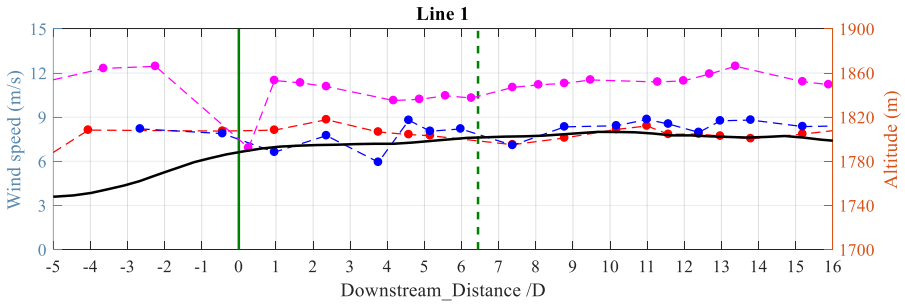


(b)

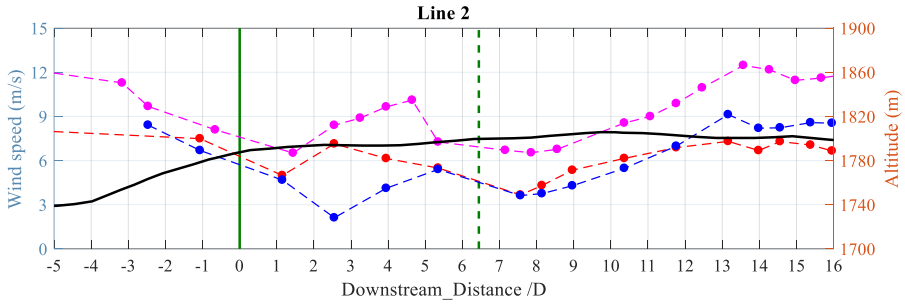

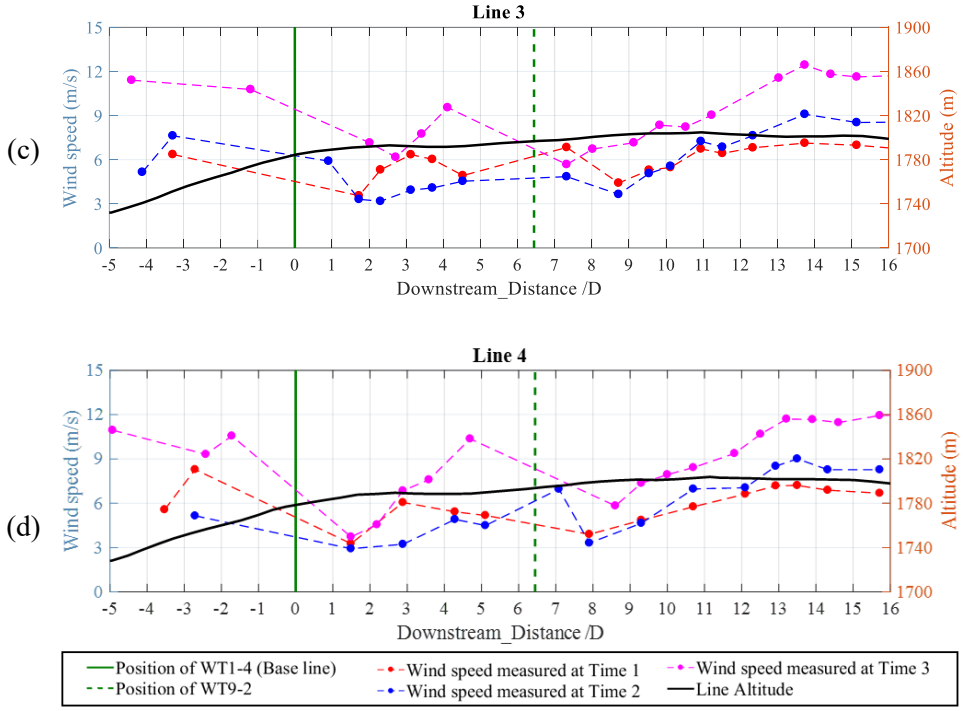


Figure 11 Measured wind speeds and line altitudes in the downstream direction (the upstream-and-downstream pattern experiment): (1) Line 1; (2) Line 2; (3) Line 3; and (4) Line 4.

The measured wind speeds and the altitudes in the corresponding lines in the crosswind direction behind WT1-4 are shown in Figure 12. The position of WT1-4 is set as the centerline, and the crosswind distance to the center is nondimensionalized by the ratio of turbine diameter.

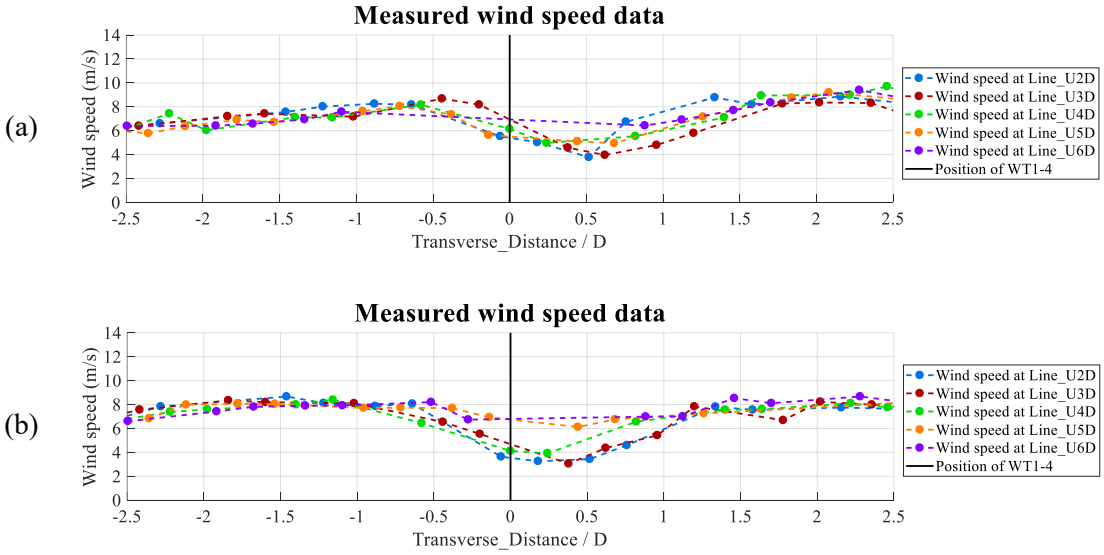

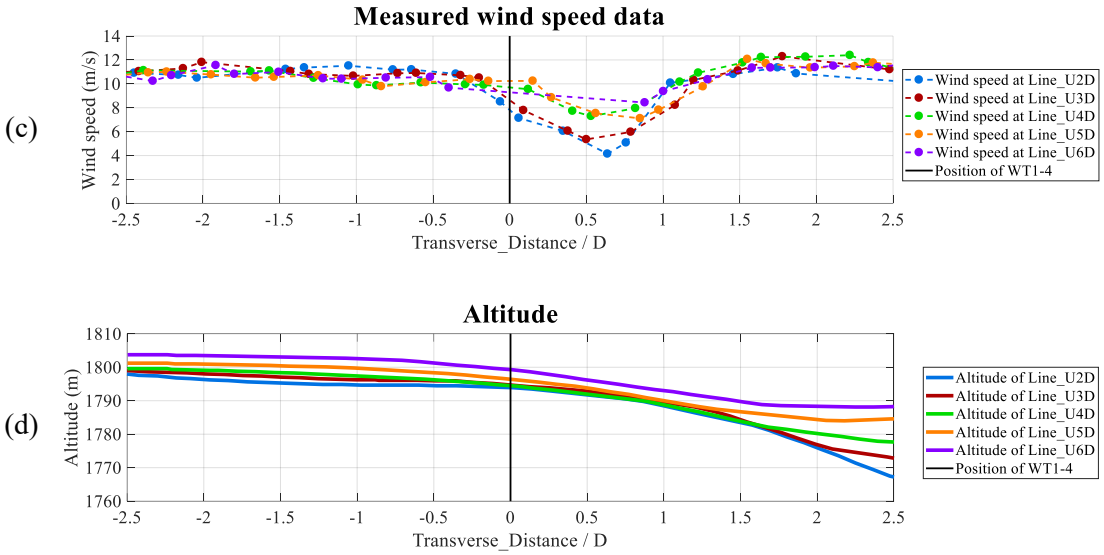


Figure 12 Measured wind speed behind WT1-4 and line altitudes (the upstream-and-stream pattern experiment): (a) Measured wind speed at Time 1; (b) Measured wind speed at Time 2; (c) Measured wind speed at Time 3; and (d) Altitude in the crosswind direction.

From the crosswind results, the largest wind deficit appeared at 2D downstream of WT1-4 at Time 3, with wind speed reducing from around 11.6 m/s to 4.1 m/s. The wake centerline is not at the position of WT1-4, and it tended to move from 0.5D to 0.8D with the increase of the downstream distance. The altitudes on the left side are similar in five lines, but they are much different from the right side 1.5D position.

The measured wind speeds and altitudes in the crosswind direction behind WT9-2 are shown in Figure 13. Similarly, the position of WT9-2 is set as the center in this case, and the crosswind distance to the center is also nondimensionalized by the ratio of turbine diameter.

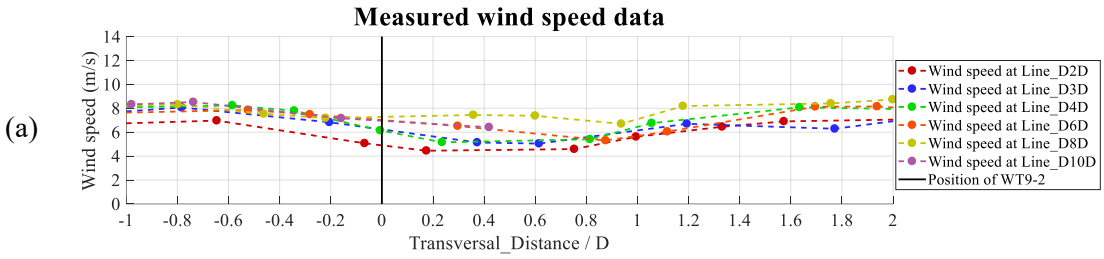

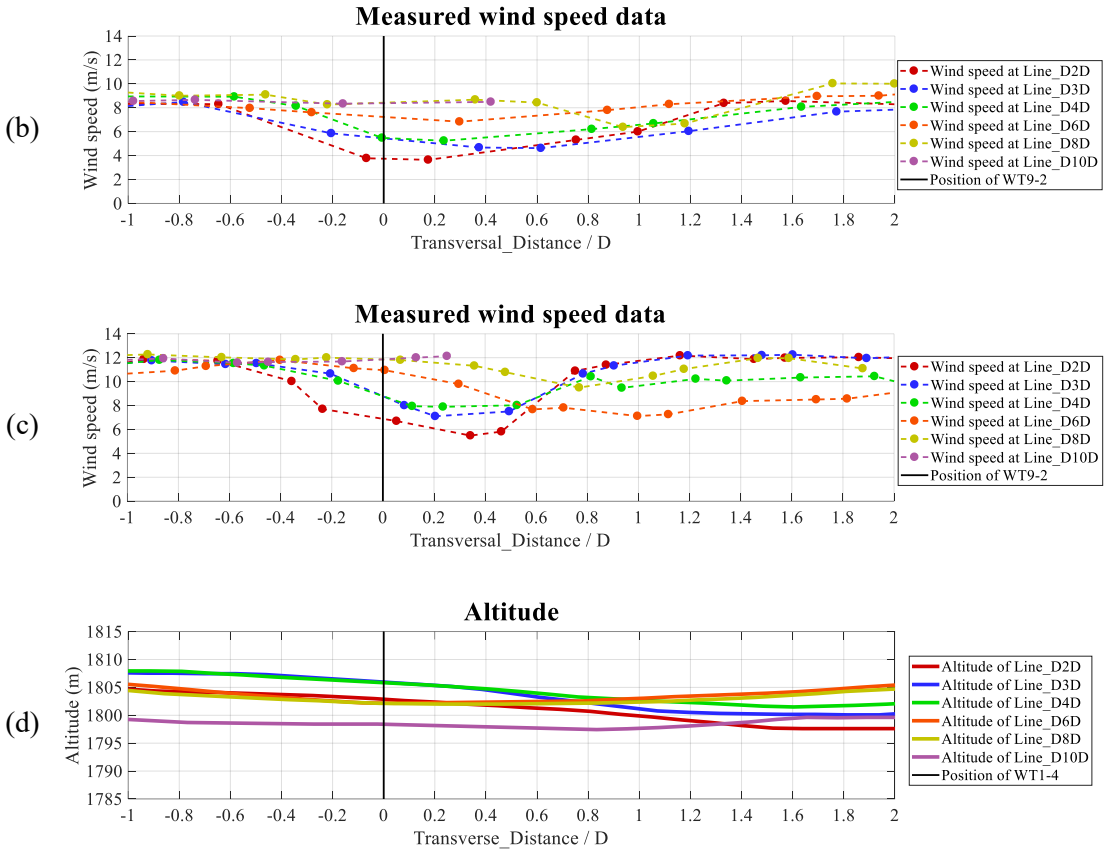


Figure 13 Measured wind speeds behind WT9-2 and line altitudes of the upstream-and-stream pattern experiment: (a) Measured wind speed at Time 1; (b) Measured wind speed at Time 2; (c) Measured wind speed at Time 3; and (d) Altitude in the crosswind direction.

As expected, the largest wind speed deficit appeared at 2D downstream of WT9-2 at Time 3, with the wind speed decreasing from around 12.0 m/s to 5.5 m/s. The range of the wake-influenced area was from -0.6D to 1.2D. As the downstream distance increased, the wake centerline continued moving right. Especially at Time 3, the centerline moved from 0.2D at 2D downstream distance to 0.8D at the 8D downstream distance in the crosswind direction. Some of the wind speed data were not available at 10D downstream distance, which was caused by the scanning limitation of Wind3D 6000. The wind deficits in the far-wake area were much smaller than those in the near-wake area. The terrain after WT9-2 is much more flat, with the maximum altitude difference of 10 m.

## 4.2 Four wind turbines in the side-by-side pattern

The second experiment is to investigate the wind distribution of turbines in a side-by-side pattern. In this experiment, four wind turbines (WT10-1, WT10-2, WT10-3, and WT10-4) have been selected, as they are fixed almost in one straight line. The positions of wind turbines and

lidars in this experiment are shown in Table 2.

Table 2 Positions of wind turbines and lidars in the side-by-side pattern experiment

| | WT10-1 | WT10-2 | WT10-3 | WT10-4 | Wind3D 6000 | WP350 |
|---|---|---|---|---|---|---|
| Longitude | 114.354838˚ E | 114.358255˚ E | 114.361603˚ E | 114.364788˚ E | 114.364677˚ E | 114.357298˚ E |
| Latitude | 40.998869˚ N | 40.998280˚ N | 40.998293˚ N | 40.997852˚ N | 40.987484˚ N | 40.999399˚ N |
| Altitude | 1857.4 m | 1884.5 m | 1880.7 m | 1877.3 m | 1814.5 m | 1872.3 m |

PPI scanning mode was also applied in this experiment. The positions of two lidars and four target wind turbines are demonstrated in Figure 14. The sector enclosed by red lines represents the scanning area of Wind3D 6000.

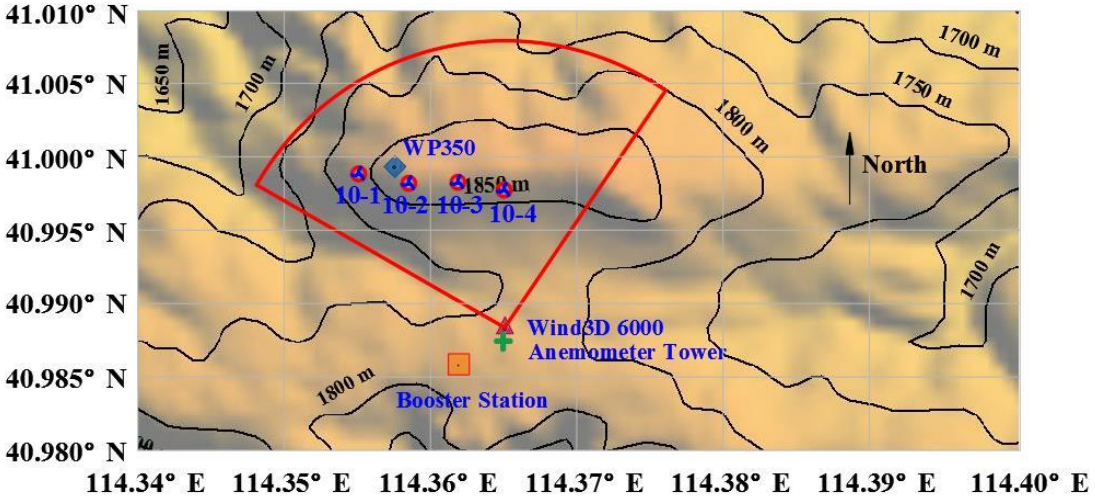


Figure 14 The positions of lidars and wind turbines in the side-by-side pattern experiment.

In this experiment, the effective results are supposed to be selected when four wind turbines were operating simultaneously, and no turbine was under the wake effect of other turbines. The steady wind should also last long enough, and the aerosol concentration must be within the operating ranges of lidars. The most ideal location for WP350 to record the inflow was the position north of the middle point of WT10-2 and WT10-3. However, due to the fens and obstacles in the wind farm, the best position cannot be achieved. Therefore, a position in front of WT10-2 was chosen. Figure 15 demonstrates the schematic diagram of Wind3D 6000 testing in the field. Four turbines are enclosed by the yellow line, whereas Wind3D 6000 is enclosed by the red line.

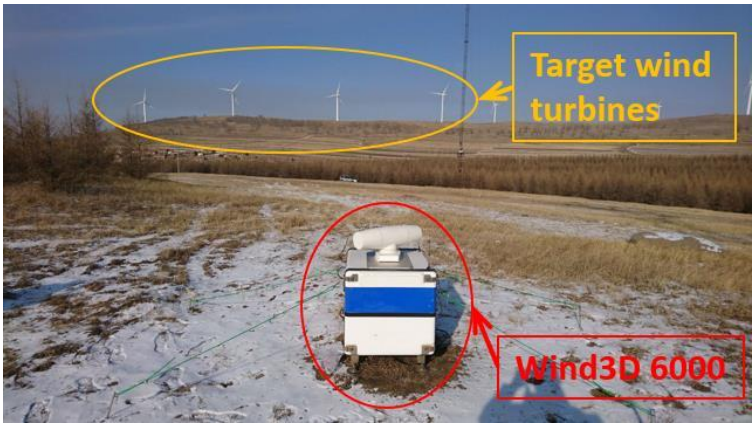


Figure 15 Schematic diagram of Wind3D 6000 testing in the field.

Four qualified periods are chosen, which are: Time 1: 6:28, March 16th, 2019; Time 2: 19:25, March 26th, 2019; Time 3: 3:38, March 27th, 2019; and Time 4: 4:14, March 27th, 2019. The inflow wind speeds and wind directions of these selected periods measured by WP350 are shown in Figure 16. The wind directions were centralized and changed in the range of 330-360°. Roughly, the wind speeds increased in the vertical direction.

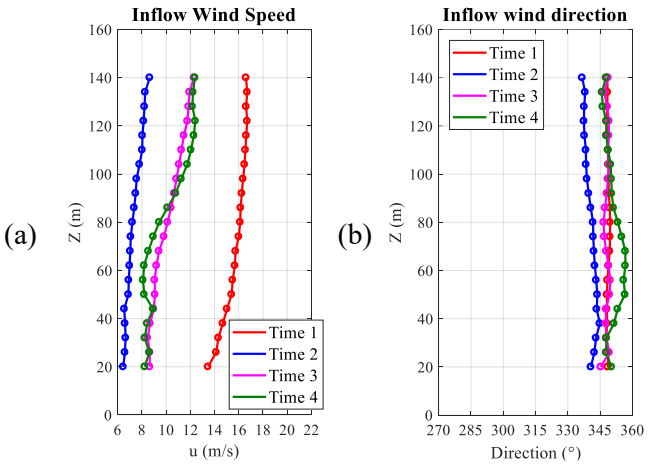


Figure 16 Inflow wind of the side-by-side pattern experiment: (a) wind speed; and (b) wind direction.

The wind speed scanning results of the plane that passes through the hub height of WT10-2 are shown in Figure 17. Four selected wind turbines were in the scanning zone of Wind3D 6000, which have been marked with black spots. During these periods, the wind directions were near northwest, and all four turbines had wakes behind themselves. The wakes were independent at the beginning and may have some interactions at the positions of long

downstream distance.

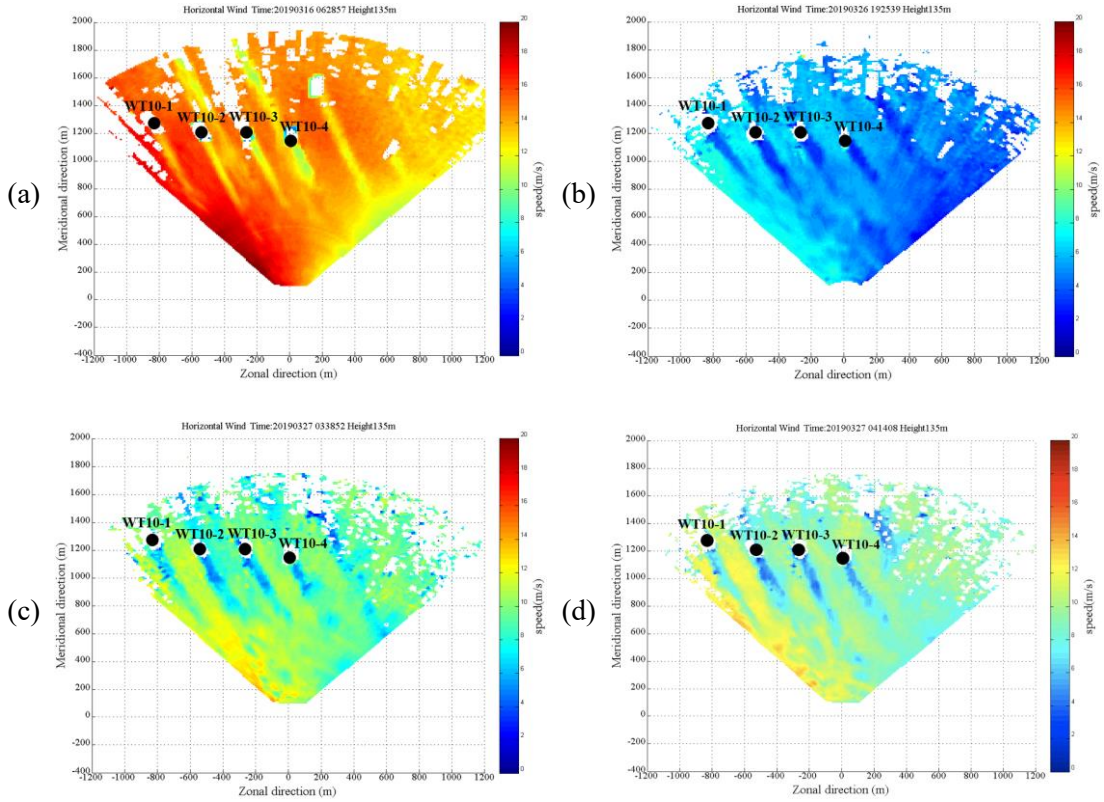


Figure 17 PPI scanning results in the plane through the hub height of WT1-4 (the side-by-side pattern experiment): (a) Time 1; (b) Time2; (c) Time 3; and (4) Time 4.

Similar to the upstream-and-downstream pattern experiment, an analyzing process has also been done for the side-by-side pattern experiment. Wind speed data are filtered based on four downwind lines and ten crosswind analyzing lines, as shown in Figure 18. Line 1, Line 2, Line 3, and Line 4 are in the wake directions and pass through WT10-1, WT10-2, WT10-3, and WT10-4, respectively. The Baseline is a line fitted by four wind turbines, and it passes through the location of WT10-2. Line_1D to Line_10D are ten lines parallel to Baseline and are applied to analyze the wind speed in crosswind sections with different downstream distances. The distance from Baseline to Line _1D is 1D, and the spacing between any other two adjacent lines is 1D as well.

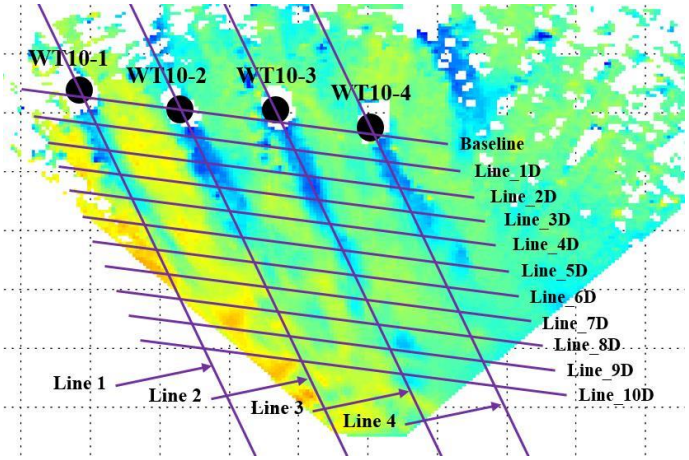


Figure 18 Diagram of analyzing lines of the side-by-side pattern experiment.

The wind speed data and the corresponding altitudes in the four lines in the downstream direction are demonstrated in Figure 19. The Baseline represents the wind turbine position, which is shown in the figure as well.

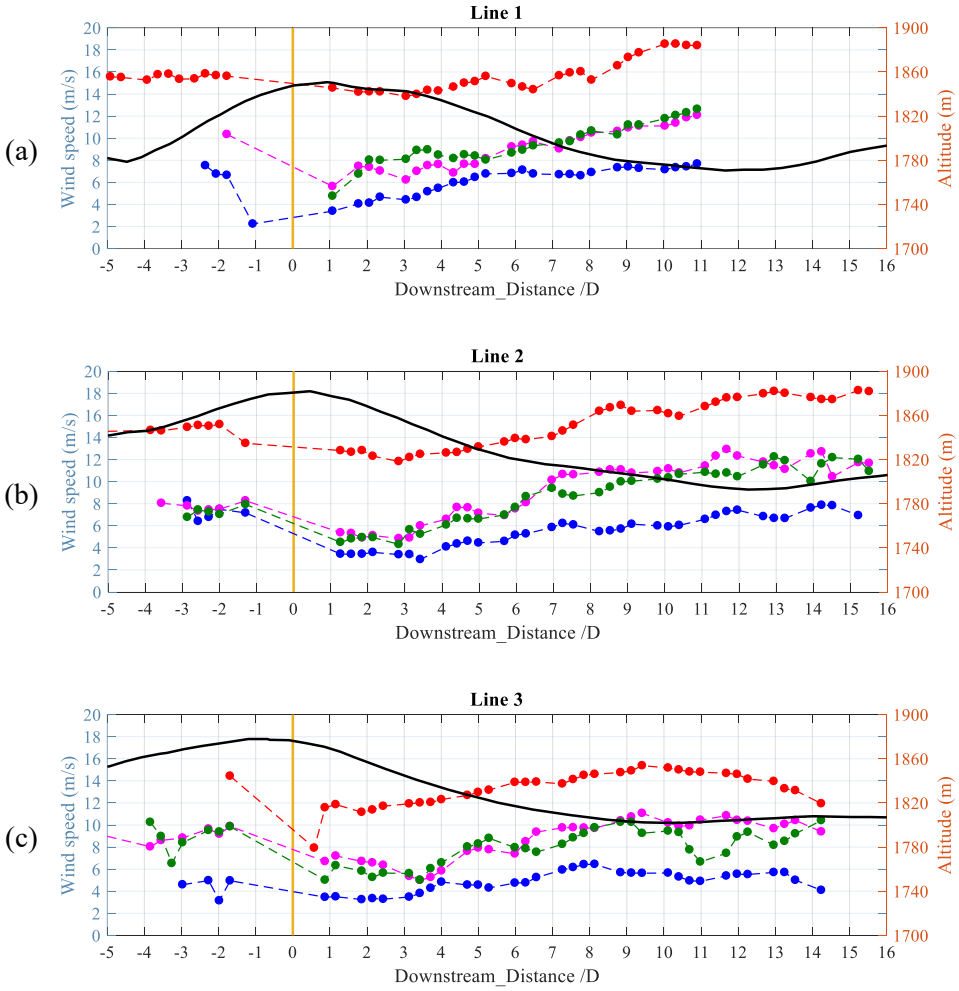

(d)

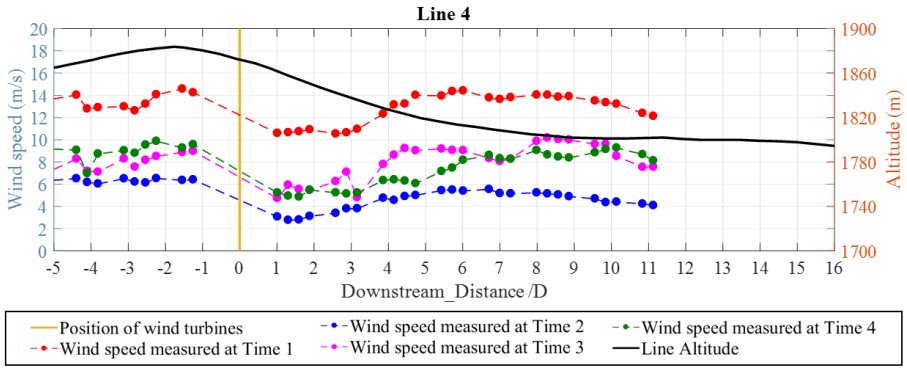


Figure 19 Measured wind speeds and line altitudes in the downstream direction (the side-by-side pattern experiment): (1) Line 1; (2) Line 2; (3) Line 3; and (4) Line.

In all four lines, huge deficits of wind speed happened right behind the wind turbines. The inflow wind was largest at Time 1. The maximum wind speed reductions in four lines were from 15.8 m/s to 14.5 m/s, from 13.7 m/s to 14.2 m/s, from 14.4 m/s to 8.0 m/s, and from 12.8 m/s to 10.6 m/s, respectively. The inflow wind was minimal at Time 2. The maximum wind speed reductions in four lines were from 2.2 m/s to 3.6 m/s, from 3.7 m/s to 7.2 m/s, from 5.1 m/s to 3.7 m/s, and from 6.3 m/s to 3.2 m/s, respectively.

The measured wind speeds in the crosswind direction behind four wind turbines are shown in Figure 20. The positions of turbines are marked as dash lines in the figure. A middle point between WT10-2 and WT10-3 is set as the original point in the crosswind direction. The crosswind distances to the original point are nondimensionalized by the ratio of turbine diameter.

(a)

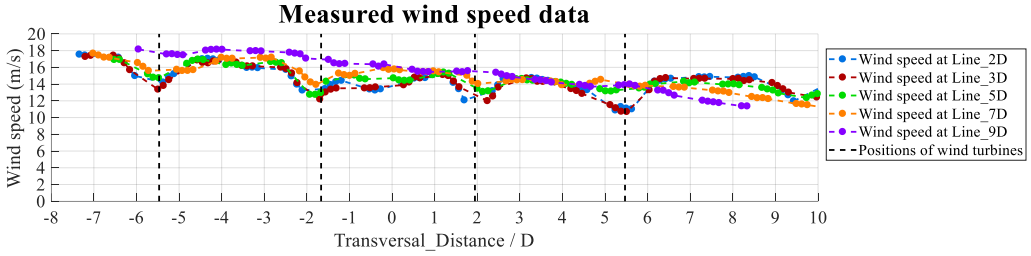


(b)

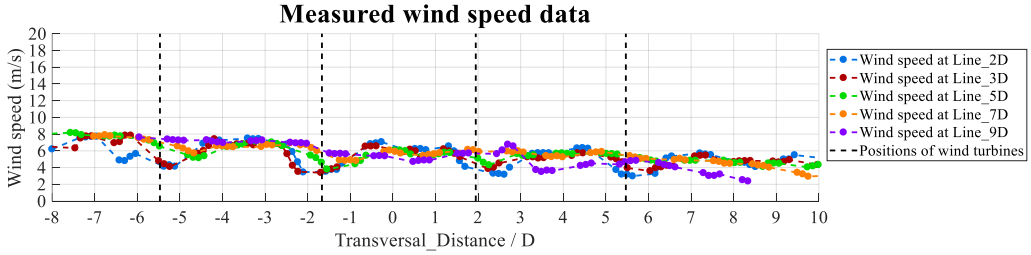

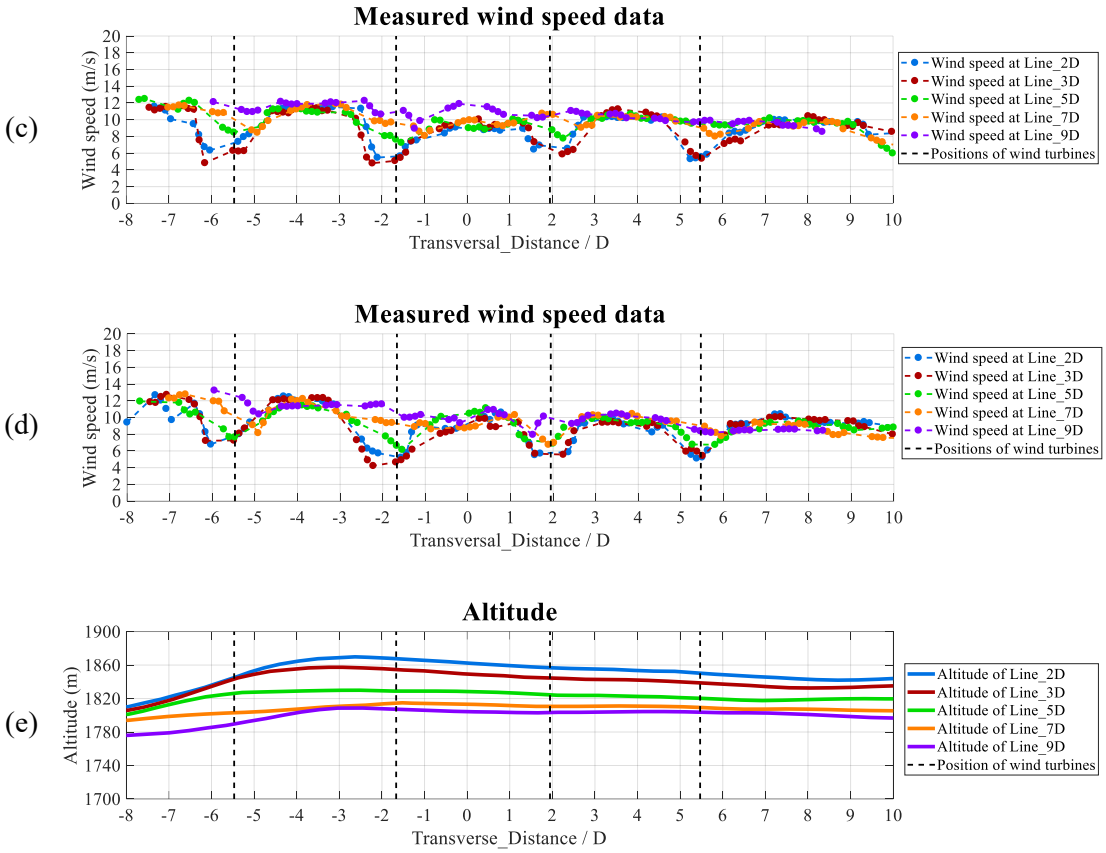


Figure 20 Measured wind speed and line altitudes of the side-by-side pattern experiment: (a) Measured wind speed at Time 1; (b) Measured wind speed at Time 2; (c) Measured wind speed at Time 3; (d) Measured wind speed at Time 4; and (e) Altitude in the crosswind direction.

From the above figures, the inflows of four wind turbines were pretty different. A decreasing trend of wind speed from WT10-1 to WT10-4 was observed. It had a close relationship with the typical topography that the terrain increases from the left side to the middle of WT10-1 and WT10-2 and then decreases to the right side. The deficit of wind speed was the largest in the near-turbine zone and decreased with the downstream distance increasing. The largest wind deficit occurred on the left side of WT10-2, with wind speed reducing from 12.4 m/s to 4.2 m/s in Time 4. The wind deficit could not be ignored even as far as 9D downstream distance. The analyzing lines generally coincided well with wake centerlines of WT10-3 and WT10-4, with only a slight difference in lines of WT10-1 and WT10-2.

To study the spatial wind distribution, more wind data from different heights should be involved. Figure 21 demonstrates the wind speeds measured at four heights of 65 m, 100 m, 135 m, and 170 m at a series of downwind distances from 2D to 9D. The measured time is 4:14

am, March 27th, 2019.

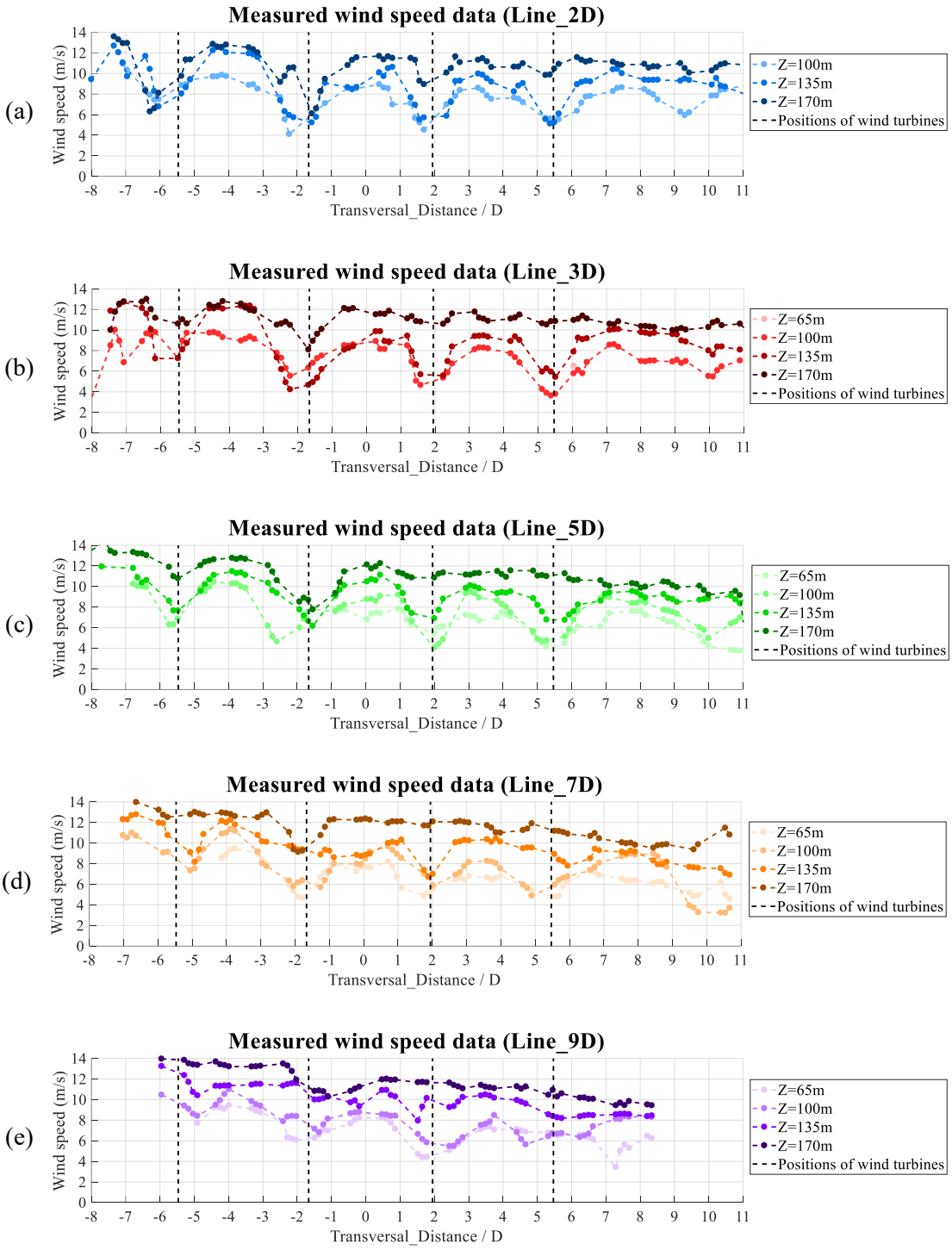


Figure 21 Measured wind speeds in different heights: (a) Line_2D; (b) Line_3D; (c) Line_5D; (d) Line_7D; and (e) Line_9D (Time: 4:14 am, March 27th, 2019).

The limitation of the scanning space of Wind3D 6000 led to the fact that the wind data

measured at the 2D downstream distance involved only three heights. This was also the reason why there were few data at 3D downstream distance at the height of 65 m and why the range of wake in the crosswind direction at 9D downwind distance was much smaller than those at other downwind distances.

During most of the experimental time, wind speeds at higher positions tended to be larger than those at lower positions. However, there were some exceptions that wind speeds did not increase with height. For example, at WT10-4 position in Line_9D, the wind speed at 65m was higher than that at 100 m. Similar phenomena were also found at all turbines positions in Line_2D, WT10-1 and WT10-3 positions in Line_3D, WT10-2 and WT10-4 positions in Line_5D, and WT10-2 position in Line_7D. All these positions are around turbines, which also indicates the complex impact of turbines on the wake distributions.

## 4.3 Analysis of the effect of complex terrains

The terrain of the upstream-and-downstream experiment is not extremely complex. Overall, the terrain on the right side is lower than that on the left side and is undulating in the downwind direction. Meandering ridges exist in this area. The terrain rises behind the upstream turbine, with the maximum elevation difference of more than 30 m.

From this experiment, firstly, the results meet well with the expectations in some aspects. The maximum deficit of wind speed occurred in the near-turbine zone and decreased with the downstream distance increasing. The wake width varied in the downwind direction, of which the overall trend is to increase gradually. Secondly, the topographical condition has a considerable effect on the wake distribution. The uneven ground makes the downstream wake more complicated. The variation of the terrain causes the corresponding change in the wake centerlines. The terrain slope and local obstacles were the main reasons for the asymmetry of wake distribution about the centerline. Thirdly, new findings have been pointed out that the wake centerlines of upstream and downstream wind turbines may be different. Under this circumstance, even though the downstream turbine is under the wake effect of the upstream turbine, the wind deficit of the downstream one is not as large as expected, and the most serious wind deficit might appear before the downstream turbine.

The topographical condition for the side-by-side pattern experiment is more complex. The three left wind turbines are installed on the top of ridges, whereas WT10-4 is installed behind the top of the ridge. The incoming wind of WT10-4 is partly blocked by the terrain. This can explain why the wind speeds before WT10-4 were pretty large, and why the ambient winds were smaller than those in the other three analyzing lines. The rising terrain leads to an uneven

speed-up before the turbine locations, which could be found in Lines 2-4.

From the side-by-side pattern experiment, apart from the similar conclusions drawn from the previous experiment, there are also some new important conclusions. Firstly, the wind instability had been observed when downstream winds restoring to the ambient wind speeds. The wind variations were extremely obvious in the far-wake zone. Referring to Figure 17, the wakes became weaker and more unstable in the far-wake zone, which may be caused by the rotations of wind turbines. The interactions between wakes and the ambient winds were pretty unstable as well. It is also hard to determine the wake width, especially in the far-wake zone, where the wakes of adjacent turbines have complicated interactions. Secondly, in the vertical direction, the change of wind speed in the wake is more obvious than the change in the ambient wind. For example, the range of wind speeds in Line 1 (the most left dotted line in Figure 20 (d)) was from 7.3 m/s to 13.0 m/s, whereas at the -4D transversal position, the range was from 11.2 m/s to 12.2 m/s. Similar phenomena could be found in other analyzing lines and transversal positions. Sometimes, wind speeds do not increase in the vertical direction where it is near the turbines. The reduced wind speeds then restore to the ambient wind beyond the wake zone. All these facts indicate that the wind turbine undoubtedly has a huge impact on the wake distribution in the downwind direction. Therefore, attention should be paid to the complex impact of the wind turbine on the wake distribution, especially in the position right behind the wind turbine.

## 5. Conclusions

In this paper, wind field experiments have been carried out to analyze and better understand the wake effect in complex terrains. The work reported in this paper is summarized as follows:

Firstly, the site and layout of the tested wind farm were introduced. Shiren wind farm is located on a complex hilly terrain in northern China, where the wind resources are relatively rich. It has a capacity of 75 MW and consists of 50 numbers of 1.5MW wind turbines. The maximum altitude difference of wind turbines in the farm is 171.3 m, with the highest wind turbine installed at the height of 1894.1 m and the lowest one installed at the height of 1722.8 m. Shiren wind farm is a good representative of a complex-terrain wind farm, of which the measured wind data deserve investigating in depth.

Two lidars were applied in the experiments. WindMast WP350 is a vertical lidar, which was used to measure the inflow before a target wind turbine. The wind speed and wind profile can be continuously detected with 30 height gates from 20 m to 350 m above the lidar. Wind3D

6000 is three-dimensional scanning lidar. It was used to capture the wake development behind the tested wind turbines. Both two lidars had been calibrated by the anemometer tower in the wind farm before they were applied in the experiments.

The experiments of two clusters of wind turbines have been conducted. One experiment included two wind turbines in the upstream-and-downstream layout pattern. This experiment aimed to investigate the influence of the upstream wind turbine on the downstream wind turbine. Data were collected when WT9-2 was right under the wake effect of WT1-4. Another experiment included four wind turbines in the side-by-side layout pattern. This experiment aimed to investigate the wake development behind a row of wind turbines. The effective results were selected when four wind turbines were operating simultaneously, and no turbine was under the wake effect of other turbines. The steady wind should last long enough, and the aerosol concentration should be within the operating ranges of lidars as well.

In the first experiment, the altitude difference is less than 10 m, indicating the terrain is not extremely complex and it may not have huge effect on the wake distribution. The observed results agreed with the previous studies that the wake width increases and the maximum wind speed deficit in each crosswind line gradually decreases in the downstream direction. The wake centerlines of the upstream and downstream wind turbines may be different, which can lead the wind deficit of the downstream turbine to be not as large as expected. In the second experiment, the terrain is much more complex, which had a huge effect on wind speed deficits, wake centerlines, and restoring wind speeds. From this experiment, obvious wind speed deficits occurred right behind the wind turbines. The wind speeds reduced mostly from 14.4m/s to 8.0 m/s in the downwind direction and from 12.4 m/s to 4.2 m/s in the crosswind direction. In the far-wake zone, wind speeds were observed to be unstable, also the wake width was not easy to be determined, because the wakes of adjacent turbines usually had complicated interactions.

In conclusion, the experimental investigation presented in this study has provided a better understanding of the wind turbine wake characteristics. The complex terrain makes the wake distribution more complicated. However, not much of the terrain factors have been involved in this study yet. Therefore, more studies will be conducted in the future focusing on how terrains influence the wake effect.

## Acknowledgement

The work described in this paper was supported by the Research Institute for Sustainable Urban Development (RISUD) with account number of BBW8, the FCE Dean Research project with account number of ZVHL, The Hong Kong Polytechnic University, and National Natural

Science Funds of China with grant number of 51606068.

## References


[1] H. Sun, H. Yang, and X. Gao, "Investigation into spacing restriction and layout optimization of wind farm with multiple types of wind turbines," *Energy,* vol. 168, pp. 637-650, 2019/02/01/ 2019.

[2] H. Sun and H. Yang, "Study on an innovative three-dimensional wind turbine wake model," *Applied Energy,* vol. 226, pp. 483-493, 2018/09/15/ 2018.

[3] R. J. Barthelmie, K. S. Hansen, and S. C. Pryor, "Meteorological Controls on Wind Turbine Wakes," *Proceedings of the Ieee,* vol. 101, no. 4, pp. 1010-1019, Apr 2013.

[4] H. Sun, X. Gao, and H. Yang, "Investigation into offshore wind farm repowering optimization in Hong Kong," *International Journal of Low-Carbon Technologies,* vol. 14, no. 2, pp. 302-311, 2019.

[5] E. Machefaux *et al.*, "An experimental and numerical study of the atmospheric stability impact on wind turbine wakes," *Wind Energy,* vol. 19, no. 10, pp. 1785-1805, Oct 2016.

[6] A. A. Veisi and M. H. Shafiei Mayam, "Effects of blade rotation direction in the wake region of two in-line turbines using Large Eddy Simulation," *Applied Energy,* vol. 197, pp. 375-392, 7/1/ 2017.

[7] H. Sun and H. Yang, "Numerical investigation of the average wind speed of a single wind turbine and development of a novel three-dimensional multiple wind turbine wake model," *Renewable Energy,* vol. 147, pp. 192-203, 2020/03/01/ 2020.

[8] Q. Li, T. Maeda, Y. Kamada, and Y. Hiromori, "Investigation of wake characteristic of a 30 kW rated power Horizontal Axis Wind Turbine with wake model and field measurement," *Applied Energy,* vol. 225, pp. 1190-1204, Sep 2018.

[9] J. J. Trujillo, F. Bingöl, G. C. Larsen, J. Mann, and M. Kühn, "Light detection and ranging measurements of wake dynamics. Part II: two‐dimensional scanning," *Wind Energy,* vol. 14, no. 1, pp. 61-75, 2011.

[10] X. Gao, H. Yang, and L. Lu, "Study on offshore wind power potential and wind farm optimization in Hong Kong," *Applied Energy,* vol. 130, pp. 519-531, 2014.

[11] X. L. Yang, M. Pakula, and F. Sotiropoulos, "Large-eddy simulation of a utility-scale wind farm in complex terrain," *Applied Energy,* vol. 229, pp. 767-777, Nov 2018.

[12] R. J. Barthelmie *et al.*, "3D WIND AND TURBULENCE CHARACTERISTICS OF THE ATMOSPHERIC BOUNDARY LAYER," *Bulletin of the American Meteorological Society,* vol. 95, no. 5, pp. 743-+, May 2014.

[13] P. B. S. Lissaman, T. G. Zambrano, and G. W. Gyatt, "Wake structure measurements at the Mod-2 cluster test facility at Goodnoe Hills," Article 1983.

[14] J. Cleijne, "Results of sexbierum wind farm: single wake measurements," 1993.

[15] W. Schlez, A. Tindal, and D. Quarton, "GH wind farmer validation report," Garrad Hassan and Partners Ltd, Bristol,2003.

[16] L. A. H. MacHielse, P. J. Eecen, H. Korterink, S. P. Van Der Pijl, and J. G. Schepers, "ECN test farm measurements for validation of wake Models," in *European Wind Energy Conference and Exhibition 2007, EWEC 2007*, 2007, vol. 1, pp. 172-181.

[17] D. A. Rajewski *et al.*, "Crop wind energy experiment (CWEX): observations of surface-layer, boundary layer, and mesoscale interactions with a wind farm," *Bulletin of the American Meteorological Society,* vol. 94, no. 5, pp. 655-672, 2013.

[18] M. E. Rhodes and J. K. Lundquist, "The effect of wind-turbine wakes on summertime US midwest atmospheric wind profiles as observed with ground-based doppler lidar," *Boundary-Layer Meteorology,* vol. 149, no. 1, pp. 85-103, 2013.

[19] B. J. Vanderwende, J. K. Lundquist, M. E. Rhodes, E. S. Takle, and S. L. Irvin, "Observing and simulating the summertime low-level jet in central Iowa," *Monthly Weather Review,* vol. 143, no. 6, pp. 2319-2336, 2015.

[20] F. Bingöl, J. Mann, and G. C. Larsen, "Light detection and ranging measurements of wake dynamics part I: one‐dimensional scanning," *Wind Energy: An International Journal for Progress and Applications in Wind Power Conversion Technology,* vol. 13, no. 1, pp. 51-61, 2010.

[21] F. Zhao *et al.*, "Experimental study on wake interactions and performance of the turbines with different rotor-diameters in adjacent area of large-scale wind farm," *Energy,* vol. 199, p. 117416, 2020/05/15/ 2020.
[22] H. Sun, H. Yang, and X. Gao, "Study on offshore wind farm layout optimization based on decommissioning strategy," *Energy Procedia,* vol. 143, pp. 566-571, 2017.
[23] R. J. Barthelmie *et al.*, "Offshore wind turbine wakes measured by sodar," *Journal of Atmospheric and Oceanic Technology,* vol. 20, no. 4, pp. 466-477, Apr 2003.
[24] R. J. Barthelmie *et al.*, "Comparison of wake model simulations with offshore wind turbine wake profiles measured by sodar," *Journal of Atmospheric and Oceanic Technology,* vol. 23, no. 7, pp. 888-901, Jul 2006.
[25] G. C. Larsen, J. Højstrup, and H. A. Madsen, "Wind fields in wakes," in *1996 European Union wind energy conference. Proceedings*, 1996: HS Stephens & Associates.
[26] I. Katic, J. Højstrup, and N. O. Jensen, "A simple model for cluster efficiency," in *European wind energy association conference and exhibition*, 1986, pp. 407-410.
[27] S. Frandsen *et al.*, "Analytical modelling of wind speed deficit in large offshore wind farms," *Wind energy,* vol. 9, no. 1‐2, pp. 39-53, 2006.
[28] J. F. Ainslie, "Calculating the flowfield in the wake of wind turbines," *Journal of Wind Engineering and Industrial Aerodynamics,* vol. 27, no. 1-3, pp. 213-224, 1988.
[29] A. Crespo, J. Hernandez, E. Fraga, and C. Andreu, "Experimental validation of the UPM computer code to calculate wind turbine wakes and comparison with other models," *Journal of Wind Engineering and Industrial Aerodynamics,* vol. 27, no. 1-3, pp. 77-88, 1988.
[30] M. Magnusson, K. Rados, and S. Voutsinas, "A study of the flow downstream of a wind turbine using measurements and simulations," *Wind Engineering,* pp. 389-403, 1996.
[31] L. Jensen, C. Mørch, P. Sørensen, and K. Svendsen, "Wake measurements from the Horns Rev wind farm," in *European wind energy conference*, 2004, vol. 9.
[32] R. J. Barthelmie *et al.*, "Modelling and Measuring Flow and Wind Turbine Wakes in Large Wind Farms Offshore," *Wind Energy,* vol. 12, no. 5, pp. 431-444, Jul 2009.
[33] R. J. Barthelmie, S. T. Frandsen, M. N. Nielsen, S. C. Pryor, P. E. Rethore, and H. E. Jorgensen, "Modelling and measurements of power losses and turbulence intensity in wind turbine wakes at Middelgrunden offshore wind farm," *Wind Energy,* vol. 10, no. 6, pp. 517-528, Nov-Dec 2007.
[34] S.-H. Kim, H.-K. Shin, Y.-C. Joo, and K.-H. Kim, "A study of the wake effects on the wind characteristics and fatigue loads for the turbines in a wind farm," *Renewable Energy,* vol. 74, pp. 536-543, 2// 2015.
[35] P. Doubrawa, R. J. Barthelmie, H. Wang, S. C. Pryor, and M. J. Churchfield, "Wind Turbine Wake Characterization from Temporally Disjunct 3-D Measurements," *Remote Sensing,* vol. 8, no. 11, Nov 2016, Art. no. 939.
[36] R. J. Barthelmie, S. C. Pryor, N. Wildmann, and R. Menke, "Wind turbine wake characterization in complex terrain via integrated Doppler lidar data from the Perdigao experiment," in *Journal of Physics: Conference Series*, 2018, vol. 1037.
[37] N. Vasiljević *et al.*, "Perdigão 2015: methodology for atmospheric multi-Doppler lidar experiments," *Atmospheric Measurement Techniques,* vol. 10, no. 9, pp. 3463-3483, 2017.
[38] X. Gao *et al.*, "Investigation of wind turbine performance coupling wake and topography effects based on LiDAR measurements and SCADA data," *Applied Energy,* vol. 255, p. 113816, 2019/12/01/ 2019.
[39] H. Sun, X. Gao, and H. Yang, "Validations of three-dimensional wake models with the wind field measurements in complex terrain," *Energy,* vol. 189, p. 116213, 2019/12/15/ 2019.
[40] X. Gao *et al.*, "Investigation and validation of 3D wake model for horizontal-axis wind turbines based on filed measurements," *Applied Energy,* vol. 260, p. 114272, 2020/02/15/ 2020.